

## Spatial Mode Control of Radiation Generated by Frequency Difference in Periodically Poled Crystals

G. Giusfredi,<sup>1</sup> D. Mazzotti,<sup>1,2,\*</sup> P. Cancio,<sup>1</sup> and P. De Natale<sup>1</sup>

<sup>1</sup>*Istituto Nazionale di Ottica Applicata (INOA), Largo Fermi 6, I-50125 Firenze, Italy*

<sup>2</sup>*European Laboratory for Nonlinear Spectroscopy (LENS) and Istituto Nazionale per la Fisica della Materia (INFN), Largo Fermi 2, I-50125 Firenze, Italy*

(Received 16 March 2001; revised manuscript received 12 June 2001; published 23 August 2001)

We demonstrate the possibility to control the spatial mode of a narrow-linewidth, continuous-wave, infrared radiation beam generated by difference frequency in a periodically poled crystal. This can be achieved by acting directly on a few experimental parameters. We show that hollow beams can be generated. A numerical routine has been developed and results agree with experimental observations, without requiring any free parameters. The relevance of these results for high-resolution spectroscopy and atom manipulation is discussed.

DOI: 10.1103/PhysRevLett.87.113901

PACS numbers: 42.60.Jf, 42.65.Ky, 42.72.Ai, 42.50.Vk

Generation of radiation by nonlinear processes has received a strong impulse by recent rapid advances in solid-state lasers as well as in nonlinear optical materials technology. In particular, difference-frequency generation (DFG) in periodically poled materials has already proven to be a unique tool for high-resolution spectroscopy [1,2].

For spectroscopic applications, wide tunability, narrow-linewidth, low-noise, and mode-hop-free operation are more important than high power and can be obtained using DFG [3]. Sub-Doppler molecular lines using a DFG-based spectrometer have been recently observed in our group, at a power as low as 10  $\mu$ W [4].

Stringent tests of fundamental physical principles can be performed with high-sensitivity spectrometers. Recently, an upper limit of  $1.7 \times 10^{-11}$  to the validity of the symmetrization postulate of quantum mechanics has been set by using difference-frequency-generated radiation [5].

However, high-resolution and high-sensitivity applications of these sources require complete control of the spatial mode of the emitted radiation. This can be important when nonlinearly generated radiation is propagated for very long distances, as in multiple-pass cells, in order to increase detection sensitivity. Excitation of very narrow molecular transitions, e.g., in the transit-time-limited regime [6], as well as efficient coupling to high-finesse cavities, critically depends on full control of spatial beam profiles.

Optical pattern formation in nonlinear materials has been extensively studied, especially from the theoretical point of view [7,8]. However, in the important case of continuous-wave (cw) DFG, to our knowledge, no systematic analysis has been performed, to date.

In this paper we report a detailed experimental study of spatial pattern evolution for infrared (IR) radiation, tunable around 4.25  $\mu$ m. This radiation was generated in a single-pass scheme, by DFG from a quasi-phase-matched periodically poled LiNbO<sub>3</sub> (PPLN) nonlinear crystal (17.5 mm long). In order to have full control of the spatial emission

mode, the pattern dependence on several experimental parameters, such as optical alignment and overlap of pump and signal beams, crystal incidence angle, and temperature, was analyzed.

Basically, the experimental setup [3] is composed of two main laser sources: a semiconductor diode laser (150 mW maximum power) emitting tunable radiation around 852 nm provides the pump beam, whereas a monolithic nonplanar-ring-oscillator Nd:YAG laser (800 mW maximum power) emitting radiation at 1064 nm provides the signal beam. The two beams are focused into the PPLN crystal to waists of about 30  $\mu$ m. A second lens ( $f = 100$  mm) placed after the crystal collimates the pump, signal, and idler beams. A Ge filter removes the pump and signal and lets the much weaker idler be spatially analyzed. Pattern recording was achieved using a Nipkow disk [9], which is a much cheaper alternative, in the IR region, to CCD cameras. Our homemade Nipkow disk has two interlaced sequences of 30 circular holes of about 200  $\mu$ m diameter, with equally spaced angular positions and uniformly varying radial distances. This disk has a detection area of (10  $\times$  10) mm with a sampling of 60  $\times$  64 pixels. After the disk, a third lens focuses the sampled idler beam onto a liquid-N<sub>2</sub>-cooled photovoltaic InSb detector with a diameter of 0.6 mm. In order to remove the contribution of background thermal radiation, sinusoidal amplitude modulation of the idler beam at 15 kHz frequency is performed by modulating the drive current of the diode lasers pumping the Nd:YAG laser. The signal is demodulated by a lock-in amplifier and several beam profiles are averaged together to improve the signal-to-noise (S/N) ratio.

A comprehensive interpretation of the experimental observations requires the development of a numerical routine. We have used the following propagation equation for the field amplitude  $E_i$  of the generated idler beam along the nonlinear crystal:

$$\frac{\partial}{\partial z} E_i(\mathbf{x}) = -\frac{\alpha}{2} E_i(\mathbf{x}) + \frac{i}{2k_i} \nabla_{\perp}^2 E_i(\mathbf{x}) + \frac{i\omega_i}{cn_i} d(z) E_p(\mathbf{x}) E_s^*(\mathbf{x}) e^{i(k_p - k_s - k_i)z}, \quad (1)$$

where  $z$  is the coordinate normal to the poling planes, the indexes  $p$ ,  $s$ , and  $i$  stand for pump, signal, and idler, respectively. The first term in the second member is the linear absorption, the second one accounts for diffraction, and the third one is the nonlinear generation contribution. In this equation,  $\alpha$  represents the linear absorption coefficient and  $d(z)$  the nonlinear susceptibility with a sign-inversion period  $\Lambda = 22 \mu\text{m}$ . A nondepletion regime for the pump and signal beams is assumed and absorbing boundary conditions are adopted [10], in order to avoid spurious effects due to reflections from the walls of the simulation area. The calculation program performs a finite-differences integration of Eq. (1) using a 3D spatial grid with an elementary cell of dimensions  $x \times y \times z = (2 \times 2 \times 1.1) \mu\text{m}$  and takes into account several experimental parameters. We remark that our model has no degrees of freedom: each significant and known experimental quantity was treated as a fixed parameter.

A Gaussian beam shape is assumed both for pump and signal beams. In fact, the Nd:YAG laser emits a circularly shaped TEM<sub>00</sub> beam, whereas the intrinsic ellipticity and astigmatism of the diode laser beam are carefully corrected by use of a pair of anamorphic prisms and a cylindrical lens. The pump and signal beams are characterized by their wavelength, power, waist, and angle of incidence onto the PPLN crystal as well as spatial overlap. Corrections for the partial reflections of the beams from the crystal surfaces (not antireflection-coated) and transmission losses for the idler beam are also included. The crystal is characterized by its temperature, length, and period of the poling, whose duty cycle is assumed to be 50%. Sellmeier equations for congruent-melt LiNbO<sub>3</sub> [11] with proper parameters for the refractive index take into account its dependence on temperature and wavelength; the thermal expansion contribution is also included with linear and quadratic terms.

Experimental recordings of the far-field (FF) idler beam shape compared with calculated patterns are shown in Figs. 1, 3 (below), and 5 (below) for three crystal temperatures. The last column shows the near-field (NF) beam profiles calculated just at the exit of the crystal. The dotted lines in the NF profiles represent  $\pi$ -spaced equiphase curves. It should be noted that each picture has its own normalized grey scale: black (white) corresponds to the maximum (minimum) intensity points. The numbers inside the pictures indicate the calculated power in  $\mu\text{W}$ . Both experimental and calculated FF images show an angular area of  $(100 \times 100) \text{ mrad}$  [corresponding to  $(10 \times 10) \text{ mm}$  in the focal plane of the collimating lens], while calculated NF images show an area of  $(540 \times 540) \mu\text{m}$ . Experimental and calculated patterns exhibit a remarkable similarity at

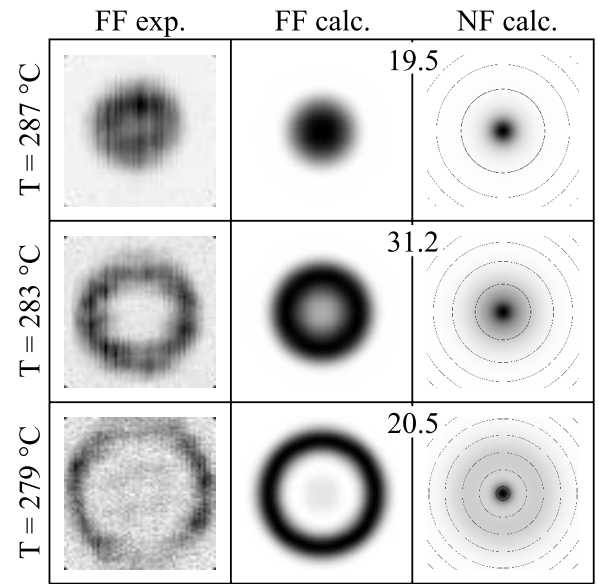


FIG. 1. Experimental recordings and computations of the beam profile for three temperatures at normal incidence (see text for details).

all temperatures, even though one obvious discrepancy is the worse contrast of the experimental recordings, due to the limitations coming from the S/N ratio. This similarity is a powerful indication of the validity of the theoretical model used where all fixed experimental parameters have been well considered.

In the case of normal incidence of both pump and signal beams ( $\theta_p \approx \theta_s \approx 0$ ), below the phase-matching temperature, a ringlike beam shape appears, whose diameter increases with decreasing temperature, as is shown in Fig. 1. The computed transverse NF beam profiles at these three temperatures, depicted in Fig. 2b, confirm that, for the lowest temperature, the idler transversal mode closely corresponds to a zero-order Bessel-Gauss beam (BGB), that is transformed into a modified BGB by the collimating lens [12–14]. Figure 2 also shows the total optical power along the crystal computed at three temperatures. It is worth noting that the maximization of the efficiency is not compatible with a TEM<sub>00</sub>-like mode requirement. Indeed, the most efficient generation is achieved when the FF beam maintains a well-visible ring shape.

We analyzed the influence of nonnormal incidence at a common angle  $\theta$  of the still overlapped pump and signal beams onto the crystal ( $\theta_p \approx \theta_s \approx \theta$ ). The results are shown in Fig. 3. It can be noticed that the BGB mode is still observed at a phase-matching temperature that decreases with increasing tilting angle. This dependence can be geometrically explained by the increase of the effective poling period with the increasing tilting angle. Figure 4 shows the noncollinear (vector) phase-matching conditions for the two cases of normal and nonnormal incidence half angle. Simple relations between the incidence angles can be derived for these two beam geometries:

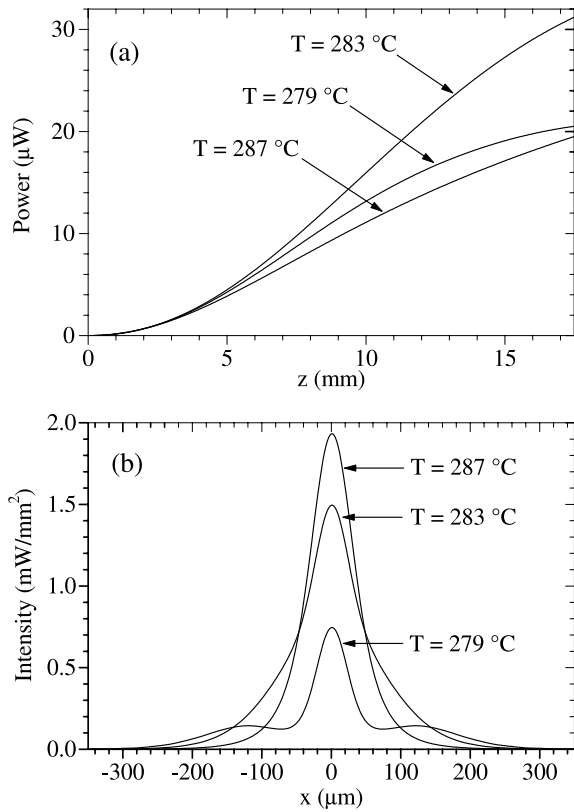


FIG. 2. Plots of computed (a) power increase along the crystal for three temperatures and (b) NF transverse beam profiles.

$$\varphi \approx n_i \arccos\left(\frac{k_p - k_s - k_c}{k_i}\right) \quad (\theta_p \approx \theta_s \approx 0), \quad (2a)$$

$$\theta \approx n_{p,s} \arccos\left(\frac{k_p - k_s - k_i}{k_c}\right) \quad (\theta_p \approx \theta_s \approx \theta), \quad (2b)$$

where the  $k$  vectors are defined by

$$k_{p,s,i}(\lambda_{p,s,i}, T) \equiv \frac{2\pi n_{p,s,i}(\lambda_{p,s,i}, T)}{\lambda_{p,s,i}}, \quad k_c \equiv \frac{2\pi}{\Lambda}. \quad (3)$$

We checked that results obtained using Eqs. (2a) and (2b) are in very good agreement with both experimental and calculated angles.

If pump and signal beams, no more overlapped, have a crossed incidence onto the crystal, the beam shape loses its rotational symmetry and becomes as in Fig. 5. The intensity of the generated beam acquires a preferential direction. An easy geometrical interpretation of this fact could be given, similar to that in Fig. 4.

The detailed characterization of the dependence of the beam shape on the experimental parameters involved in the nonlinear generation process has some direct consequences and applications. The main result is the possibility to control the beam shape by temperature and angle of

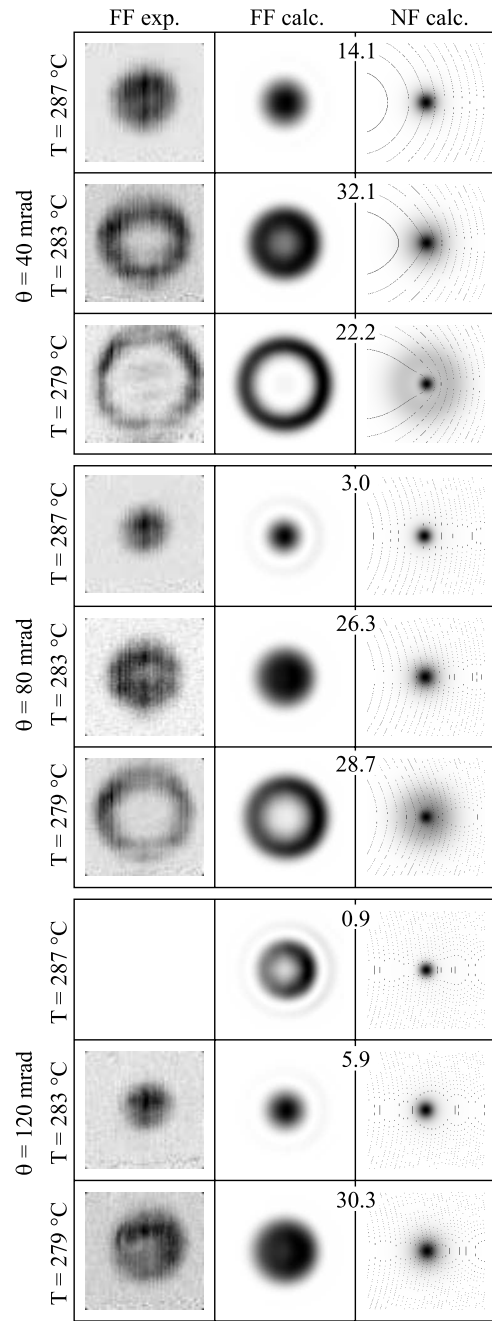


FIG. 3. Experimental recordings and computations of the beam profile for three temperatures and three nonnormal incidence angles (see text for details). The pattern at  $\theta = 120$  mrad and  $T = 287$  °C was not recorded due to its very weak intensity. The darker circle appearing in the corresponding calculated picture represents the secondary maximum of the phase-matching function, with a  $(\sin x/x)^2$  behavior.

the nonlinear crystal, using Eqs. (2a) and (3). Of course, active control of the pattern would require application of standard methods used in pattern recognition techniques. This could be important for several applications to spectroscopy and atomic physics. For example, we are building an optical enhancement cavity for the  $4.25 \mu\text{m}$  radiation

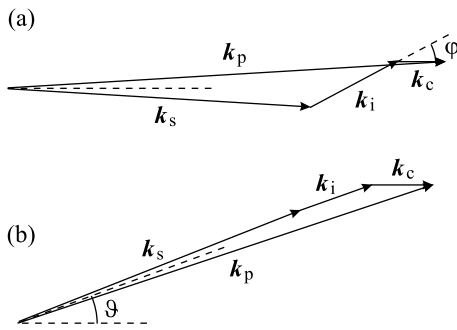


FIG. 4. Geometrical interpretation of the phase-matching conditions for overlapped pump and signal beams at (a) normal and (b) nonnormal incidence onto the crystal.

with a finesse of 500. Preliminary results show that coupling of the IR beam into the confocal Fabry-Perot cavity is strongly dependent on the mode matching between the incoming radiation and the optical cavity itself. In fact, adjusting the temperature, we measured a variation of the coupling coefficient from 75% (for a near-Gaussian beam) to about 37% (for a modified BGB).

Our analysis applies to parametric generation with a single input beam, as well. Instead, for second harmonic generation, the geometrical explanation given in Fig. 4 shows that ringlike beams can be only barely observable. This pattern analysis suggests that, beyond zeroth-order BGB, higher-order BGB can be generated, too. Indeed, if an azimuthal phase plate is placed at the second focal plane of the collimating lens, a higher-order modified BGB

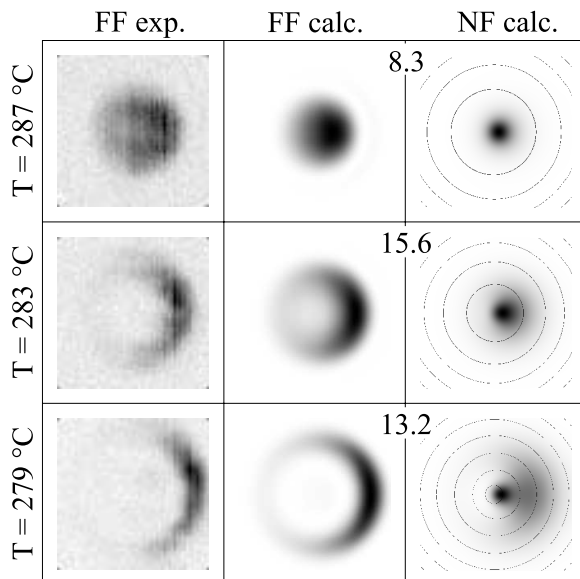


FIG. 5. Experimental recordings and computations of the beam profile for three temperatures at 10 mrad crossed incidence (see text for details).

(“optical vortex” [15]) can be generated. Hollow beams are finding increasing application for manipulation and guiding of cold atoms [16,17]. More recently, even molecules, with a rich rovibrational spectrum in the IR, have been cooled down by different techniques [18]. We have demonstrated the possibility to generate hollow beams in this wavelength region, avoiding the use of optics such as axicons, holograms, or hollow fibers. For such applications, the optical power achievable with present single-pass systems would be inadequate for confinement, although the cw generation efficiency is steadily increasing thanks to progress in nonlinear materials and high-power solid-state lasers.

D. Mazzotti thanks Agenzia Spaziale Italiana (ASI) for providing his grant. We also wish to thank M. Artoni (LENS) for a critical reading of the manuscript.

\*Email address: mazzotti@ino.it

- [1] D. Richter, D. F. Lancaster, and F. K. Tittel, *Appl. Opt.* **39**, 4444 (2000).
- [2] K. Fradkin, A. Arie, P. Urenski, and G. Rosenman, *Opt. Lett.* **25**, 743 (2000).
- [3] D. Mazzotti, P. De Natale, G. Giusfredi, C. Fort, J. A. Mitchell, and L. W. Hollberg, *Appl. Phys. B* **70**, 747 (2000).
- [4] D. Mazzotti, P. De Natale, G. Giusfredi, C. Fort, J. A. Mitchell, and L. W. Hollberg, *Opt. Lett.* **25**, 350 (2000).
- [5] D. Mazzotti, P. Cancio, G. Giusfredi, M. Inguscio, and P. De Natale, *Phys. Rev. Lett.* **86**, 1919 (2001).
- [6] W. Demtröder, *Laser Spectroscopy* (Springer-Verlag, Berlin, 1996), 2nd ed., p. 85.
- [7] F. T. Arecchi, S. Boccaletti, and P. Ramazza, *Phys. Rep.* **318**, 1 (1999).
- [8] L. A. Lugiato, M. Brambilla, and A. Gatti, *Optical Pattern Formation*, Advances in Atomic, Molecular, and Optical Physics Vol. 40 (Academic, New York, 1998), p. 229.
- [9] G. Giusfredi and R. Hostetler, *Rev. Sci. Instrum.* **60**, 598 (1989).
- [10] L. Di Menza, *J. Opt. B* **1**, 19 (1999).
- [11] D. H. Jundt, *Opt. Lett.* **22**, 1553 (1997).
- [12] F. Gori, G. Guattari, and C. Padovani, *Opt. Commun.* **64**, 491 (1987).
- [13] V. Bagini, F. Frezza, M. Santarsiero, G. Schettini, and G. Schirripa Spagnolo, *J. Mod. Opt.* **43**, 1155 (1996).
- [14] M. Santarsiero, *Opt. Commun.* **132**, 1 (1996).
- [15] P. Di Trapani, W. Chinaglia, S. Minardi, A. Piskarskas, and G. Valiulis, *Phys. Rev. Lett.* **84**, 3843 (2000).
- [16] Y. Song, D. Milam, and W. T. Hill III, *Opt. Lett.* **24**, 1805 (1999).
- [17] X. Xu, V. G. Minogin, K. Lee, Y. Wang, and W. Jhe, *Phys. Rev. A* **60**, 4796 (1999).
- [18] H. L. Bethlem, G. Berden, F. M. H. Crompvoets, R. T. Jongma, A. J. A. van Roij, and G. Meijer, *Nature (London)* **406**, 491 (2000).